Aero-Acoustic Optimization of Airfoils for Wind Turbines

Jaime F. G. Coimbra* and André C. Marta†
Center for Aerospace Science and Technology, Instituto Superior Técnico,
Av. Rovisco Pais 1, 1049-001 Lisboa, Portugal

The subject of airfoil design, in the context of wind turbines, is approached with the objective of optimizing the geometry for the best aerodynamic and aero-acoustic trade-off. The work developed is made up of four stages: the aerodynamic analysis module, which consists of two parts, one responsible for airfoil design and parameterization and another dedicated to flow analysis; an aero-acoustic module, based in the semi-empirical model from Brooks, Pope and Marcolini and the turbulent inflow prediction scheme from Moriarty, Guidati and Migliore; the integration of both modules in one single computational tool; and the development of a multi-objective optimization framework. The airfoil geometry build tool is based on the mathematical description of Bezier curves and, the wind turbine dedicated computational tool Rfoil has been used for boundary-layer modeling and inclusion of rotational effects. The code developed integrated both developed modules in a single interactive shell in Python. The Python module pyOpt was selected as the interactive development environment in which the optimization took place. A genetic algorithm was selected to handle multiple local minima and multi-objective problems. Several airfoil families, commonly used in the wind turbine technology, were analyzed from the aerodynamic and aero-acoustic perspectives with the developed tools, and used as reference for general comparison. Optimized airfoil geometries, that either minimize noise emission or favour aerodynamic performance were obtained and classes of aero-acoustically optimized airfoils were identified in the resulting Pareto fronts.

I. Introduction

Wind turbine (WT) technology has been a subject of increasing research and development in the last 30 years, for which rising environmental concerns have contributed. Presenting major technical and economical advantages, WTs have been the main selected option of several countries and entities[1] to answer to their energetic shortages or diminish fossil fuel dependency. Such is the Portuguese case, that has seen one of the biggest growths in available electrical power from wind farms in the world. That general increase is responsible for the growing exposure of people to WT noise, specifically habitants of rural or less densely populated areas where wind availability is bigger, with effects ranging from simple inconvenience to severe health problems.[2] Noise presents itself as one of the main disadvantage of WTs and should be subject to evaluation from the engineering point of view.

The main objective to be achieved here was the multi-disciplinary optimization of airfoils for wind turbines, in the specifics of the aero-acoustic subject. The relation between changes in airfoil geometry and resulting noise emission and variations in aerodynamic properties was to be studied to find families of optimized airfoils that could deliver, if possible, a better trade-off between noise and aerodynamic performance than other available airfoil geometries known to be used in the context of wind turbines technology. Several exercises, consisting of varying several parameters used to simulate different working conditions, were conducted and its effects on airfoil geometry, noise emission and aerodynamic performance were analyzed simultaneously.

*MSc Student.
†Researcher, AIAA Member.

II. Background

In this section the theoretical background for the specifics and details of the aerodynamic and aero-acoustic modules are presented and briefly discussed.

A. Aerodynamic module

The aerodynamic module is responsible for, firstly, designing and reshaping the airfoil geometries, resorting to various mathematical definitions and, secondly, for controlling the flow analysis parameters and features.

The subject of airfoil design is not new and several methods exist that are commonly used for obtaining a geometry. The reference for this are the NACA airfoils, developed mainly for aeronautics, but others specific of WT technology are available, such as the Riso[3] or the DUDELFT[4] airfoils.

The subject of airfoil parameterization is a completely different topic as several mathematical descriptions can be used to introduce shape changes in the airfoil under consideration.[5] The possibility of performing both local and global changes, with large or small effects, and the simplicity in the description compatible with code implementation, were the selection factors for this work. To this end, a description using Bezier curves was used. The mathematical description of the Bezier curves, described in the form of a 3^{rd} order curve in Eq.(1), stood out from the rest[6] for presenting major advantages for this application and receiving positive feedback from other authors.[7,8]

$$\mathbf{B}(t) = (1-t)[(1-t)\mathbf{P}_0 + t\mathbf{P}_1] + t[(1-t)\mathbf{P}_1 + t\mathbf{P}_2] \ , \ t \in [0,1] \tag{1}$$

The interpretation of the method was done here using four 3^{rd}-order Bezier curves that form an airfoil geometry in the form of four connected sectors, which are controlled by their respective control points (CP), as shown in Fig.1. The connections between curves present a major concern in the modeling tool as the first CP of a curve coincides with the last CP of the previous curve and connectivity agreement must be accounted. Also, the coordinates of the CPs, apart from the points that sit in the LE and TE positions which are fixed, are used as design variables in the optmization.

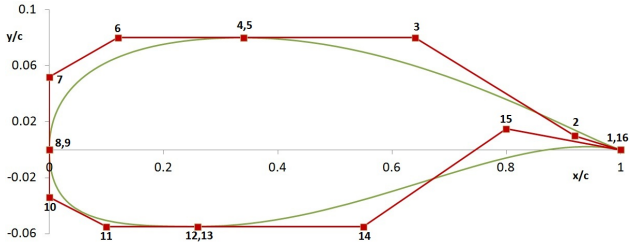

Figure 1. Airfoil surface built with four Bezier curves

The simulation of the working conditions of the airfoil were achieved using the Rfoil software,[9] an upgraded version of Xfoil,[10] which was responsible for Boundary-Layer (BL) modeling and for including the rotational effects inherent to WT standard operation. The input parameters for accounting the rotational effects are computed and selected using the blade element momentum theory (BEM). These will be used as test variables in the several optimization tests conducted.

B. Aero-acoustic module

The aero-acoustic prediction scheme developed for application in this work consists of two sub-modules. The first is based on the works developed by Brooks, Pope & Marcolini (BP&M)[11] on the subject of airfoil self-noise. The second deals with modeling the interaction of the turbulent inflow with the shape of the LE of the airfoil, as described in the works of Moriarty, Guidati & Migliore (MG&M).[12,13]

The work of BP&M consists of a series of aero-acoustic experimental tests of the NACA 0012 airfoil geometry, with which data the researchers were capable of developing a semi-empirical model for the noise prediction of five noise mechanisms, with results presented as sound pressure levels at the observer as a function of frequency for the 1/3 octave spectra. The original model could not be applied to other geometries as it only had present BL formulations for the NACA 0012 airfoil but the integration of the aerodynamic and the aero-acoustic module here developed in this work overcomes that obstacle.

The five noise mechanisms are turbulent boundary-layer trailing edge noise, separation-stall noise, laminar boundary layer vortex shedding noise, tip vortex formation noise, and trailing edge bluntness vortex shedding noise. Since only 2D flow is to be simulated, the tip vortex formation noise mechanism was discarded.

The scaling laws for the different mechanisms are all of similar form, as represented in Eq.(2),

$$SPL_i = 10\log\left(\frac{\delta_i^* Ma^{f(i)} d\bar{D}}{r_e^2}\right) + F_i(St) + G_i(Re) \tag{2}$$

where δ_i^* is the BL displacement thickness, Ma is the Mach number, $f(i)$ is the raised power which depends on the particular noise mechanism considered i ($i = 1, 2, 3, 4, 5$), d is the airfoil section semi-span, $\bar{D}$ is a sound directivity function that can take two forms for computing high or low frequency values and r_e is the source-observer distance. The additional terms $F_i(St)$ and $G_i(Re)$ represent the many spectral shape functions of the Strouhal number St and the Reynolds number Re, respectively, that differentiate the many noise mechanisms.

The work of MG&M present a numerically more detailed scheme on the subject of turbulent inflow noise prediction for any airfoil geometry, where the authors identified a linear relation between the Strouhal number and the difference in Sound Pressure Level (SPL) values (ΔSPL) relative to the known test case of a flat plate presented by Amiet,[14] from the analysis of thickness and camber distribution of several tested airfoils. Relative thickness, at 1% and 10% chord, of the LEs of the tested airfoil geometries were used to yield a simple formulation responsible for computing the ΔSPL values which, when coupled with the improved expressions of Amiet by Lowson,[15] allow for the computation of absolute SPL values of any airfoil geometry considered. Equations (3) and (4) deliver the SPL values in function of the frequency 1/3 octave spectra.

$$SPL_{Inflow} = 10\log\left(\frac{LFC}{1+LFC}\right) + SPL^H_{Inflow} \tag{3}$$

$$SPL^H_{Inflow} = 10\log\left(\frac{\rho^2 c_0^2 Ld}{r_e^2} Ma^3 U^2 \bar{u}^2 K_x^3 (1+K_x^3)^{-7/3} \bar{D}_h\right) + 58.4 \tag{4}$$

These expressions introduce several parameters related with the properties for the turbulent inflow noise, such as turbulence intensity and turbulence length scale, which are ultimately related with the height above ground and ground roughness considered.[16]

III. Implementation

In this section, major focus will be given to the multi-disciplinary and multi-objective optimization framework.

A. Genetic algorithms applied to airfoil design

Many authors choose to use mainly gradient-based optimization methods in airfoil design, whereas others present works that resorted to evolutionary based methods. In conclusion to the survey taken on some works that focused on airfoil optimization,[17] no mandatory rules exist on how to correctly approach an airfoil design optimization problem, which means it all depends on the nature the problem.

The strategy followed here needed to account for the possibility of multi-objective optimization (MOO), which was one of the main objectives, meaning that a method like genetic algorithms (GA) seems to be more suitable. These algorithms are based in the process of natural selection observed from biological life, following heuristic search patterns. The main advantages of using these algorithms is the possibility for multi-objective optimization, developing solutions that search for the global minima and the good performance delivered for optimization defined with a low number of constraints. On the downside, evolutionary algorithms may be time consuming as they require a large number of function evaluations.

B. Optimization test parameters

The test parameters used for the optimization procedures performed are selected in function of the main parameters that are expected to deliver relevant effect on the overall evolution of the optimized geometries or the values of the aerodynamic coefficients or SPL. For a correct selection of these parameters, three airfoils integrated in one of the blades of a WT were considered. The immediate parameters that will help perform a

sensitivity analysis of these effects are chord length, airfoil span, maximum relative thickness, velocity ratio and chord-to-radius ratios. The values summarized in Tab.1 were estimated based of information available on real WTs.

Table 1. Airfoil parameters considered for optimization purposes

Parameter / Airfoil	#1	#2	#3
Chord (c [m])	3.6	1.4	0.8
Airfoil Span (L [m])	7.2	2.8	1.6
Max. rel. thick. (t/c [%])	40	18	18
Radial position (r/R)	0.10	0.65	0.90
Velocity ratio (x)	0.70	4.55	6.30
Chord/Radius (c/R)	0.08182	0.03182	0.01818

C. Optimization framework

The optimization problem discussed here follows the general formulation,

$$\begin{aligned} \text{minimize} \quad & f(x) \\ \text{by varying} \quad & x \in \mathbb{R}^n \\ \text{subject to} \quad & h_p(x) = 0, \quad p = 1, 2, \ldots, N_h \\ & g_m(x) \geq 0, \quad m = 1, 2, \ldots, N_g \end{aligned} \tag{5}$$

Two objective functions are to be considered, one that maximizes the C_l/C_d ratio (f_1) and another which works to minimize total SPL values of the airfoils (f_2). The decision variables introduced in the optimization formulation, correspond to the coordinates of the CPs that define the overall surface of the geometry, along with the angle of attack. The constraints considered are mainly related with geometric issues to maintain the relative positions of each CP to each other in a way that an aerodynamic body is always designed and no irregular shapes are considered. Relative maximum thickness is limited to either 18% or 40%, depending on the radial position considered. The design space of each decision variable is set for each individual test case, but in general follow the schematics shown in Fig.2.

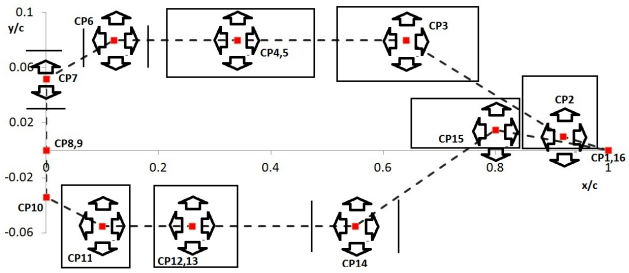

Figure 2. Example of search space and freedom of movement of the CPs

The Python library *pyOpt*[18] provided the interactive development environment to create the optimization framework and integrate the code developed in a simple optimization flow, as illustrated in Fig.3.

IV. Results

A selection of the preliminary results of some optimization tests performed, along with a discussion of the same, is presented here. The final paper will have a more comprehensive set of results and detailed discussion.

A. Code verification and validation

Code *AAcoustic* makes up for the platform where the aerodynamic and aero-acoustic modules are interpreted. The most susceptible to interpretation of the two, is the aero-acoustic module and for that reason emphasis

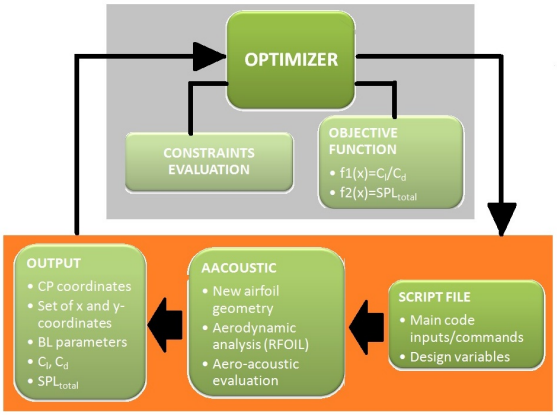

Figure 3. Optimization flow diagram

in its verification is done here. A brief discussion of the BL parameter results from Rfoil and the original expressions from[11] is performed, regarding the main test case considered for the NACA0012 reference airfoil. The algorithm used for implementing the turbulent inflow prediction scheme, based on the works of,[13] is also validated and presented.

1. *Comparison with BP&M work*

The work of BP&M is based on wind tunnel experiments and the original paper provides an extensive amount of data that can be used for verification of the code for the NACA 0012 airfoil, whose working conditions are displayed in Tab.2. The observer angles relative to the x and y-axis are Θ_e and Φ_e, respectively, α is the

Table 2. Test parameters used for reference airfoil

Airfoil	NACA 0012
c [m]	0.3048
L [m]	0.4572
r_e [m]	1.22
Θ_e [deg]	90.0
Φ_e [deg]	90.0
α [deg]	1.516
U [m s^{-1}]	71.3

angle of attack and U is the mean wind speed.

The considered noise mechanisms are the TBL-TE, separation and LBL-VS sources, while the effects of bluntness and tip noise mechanisms were discarded, as suggested in the original work. The resulting total 1/3 octave spectra of the main test case considered is presented in Fig.4, for the two algorithms developed for this purpose: the first being based in the original expressions of BP&M for BL properties computations and the second which replaces those original expressions with the results from the Rfoil software for the same properties. Although both curves follow similar trends, it is notorious the difference from the semi-empirical method (*Original BPM* line) to the computational tool (*Code (Rfoil)* line), especially in the low frequency range, which can only be related with the difference in results for the BL parameters. Nevertheless, the code developed does interpret correctly the original method, as seen from the agreement in the corresponding lines which means that, since the original expressions cannot be used for other airfoil geometries, like the ones that are designed here, the use of the Rfoil software does not compromise severely the results obtained from the code, with considerable accuracy.

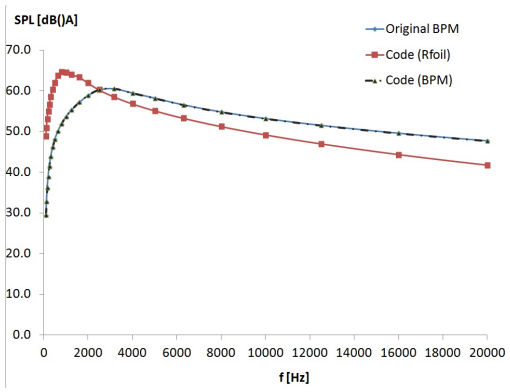

Figure 4. Results for the SPL computation of the NACA 0012 airfoil, for all airfoil self-noise mechanisms

2. *Turbulent inflow scheme*

The validation of the original method is still a subject of study nowadays and a reliable verification is quite difficult. The authors of the original method developed a code[19] in which the noise related to turbulent inflow can be estimated. This software was used as comparison for validating the algorithm here developed, but these results should be considered only in a simple qualitative form and not as absolute. The verification is processed in both codes for the same test case performed previously for the BP&M method, now accounting for only turbulent inflow noise, as illustrated in Fig.5. The results show that the code under-predicts the

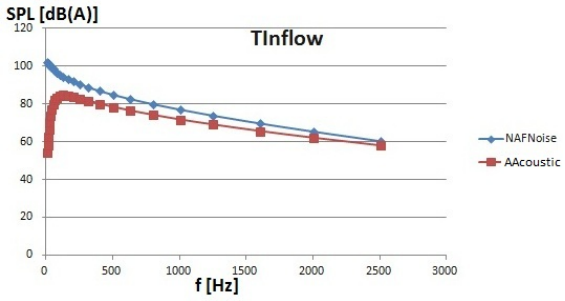

Figure 5. Results for the SPL computation for turbulent inflow noise, of the NACA 0012 airfoil

turbulent inflow noise, but with general good agreement apart from the major difference in very low frequency values, This could be related with possible different methods used in both codes to compute the required parameters of the method (namely relative LE thickness of the airfoil and the interpretation of the work of Amiet).

B. Reference airfoils

The selected airfoil geometries to represent the main airfoil families typically used in the context of WT technology are the FFA-W3-211,[3] NACA4421 and NACA63415.[20] The geometries of these airfoils are displayed in Fig.6. These airfoil geometries were considered as if integrated in a real WT and subject to

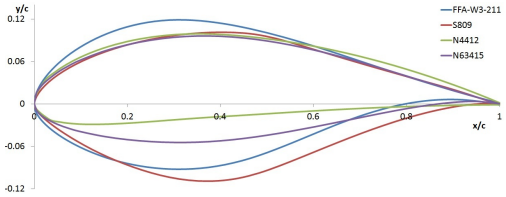

Figure 6. Geometries of the selected reference airfoils

the optimum angle of attack that either maximize C_l/C_d ratio or minimize SPL value for the conditions $U = 20[m.s^{-1}]$ and $r_e = 250[m]$. The most relevant considered parameters and results for these airfoils are displayed in Tab.3 for those conditions.

Table 3. Aerodynamic and aero-acoustic properties of several reference airfoils

Airfoil	FFA-W3-211	N4412	N63415
r/R	0.10	0.65	0.90
c [m]	3.6	1.4	0.8
x	0.7	4.5	6.3
L [m]	7.2	2.8	1.6
t/c	0.21	0.12	0.15
Ψ [deg]	16.3	15.6	14.4
C_l/C_d (α^* [deg])	165.9 (6.4^o)	143.8 (9.1^o)	125.7 (2.2^o)
SPL_T (α^* [deg])	33.8 (13.8^o)	62.0 (0.8^o)	64.2 (0.1^o)

C. Effects of the radial position

To assess the effect of considering the optimized geometries in different radial positions, the flow speed was set at $U = 20[m.s^{-1}]$ and the source-observer distance is fixed at $r_e = 250[m]$, as summarized in Tab.4.

Table 4. Constant parameters used for obtaining OptFoils 3, 7, 15, 19, 27 and 31

$U = 20[m.s^{-1}]$ $r_e = 250.0[m]$						
Parameter/OptFoil	3	7	15	19	27	31
r/R	0.10		0.65		0.90	
c [m]	3.6		1.4		0.8	
x	0.7		4.5		6.3	
L [m]	7.2		2.8		1.6	

The resulting geometries that favour aerodynamics are illustrated in Fig.7 It is immediate that C_l/C_d

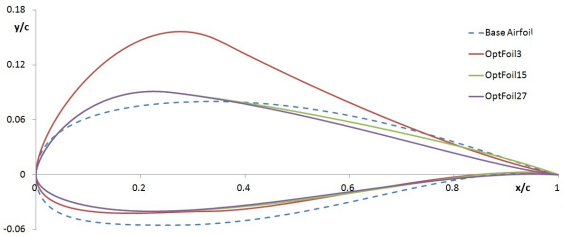

Figure 7. Optimized geometries to assess the effect of radial position on aerodynamic performance

ratios are higher for the thicker airfoils that are likely to be considered at the near root region, which is not surprising as the relative thickness accepted to constrain the optimization for the airfoils in this position was of 40%, whereas the airfoil geometries considered for the mid-span and near tip region of the blade developed less camber and fixed the point of maximum relative thickness closer to the LE. It is apparent as well that the near tip region airfoils are likely to deliver higher SPL values and that improvement in aerodynamics in comparison to the airfoils placed at mid-span is achieved by the decrease of thickness distribution near the TE, on the suction side.

The selected geometries that represent the effect of radial position, optimized to minimize SPL values are presented, in Fig.8. Again, thickness distribution is of great relevance and the thicker LE of the airfoils placed at the near root region could help explain how these airfoils radiate the least amount of noise, since this section of the geometry is directly related with one of the most relevant noise sources, turbulent inflow. More relevant to the matter are the optimized geometries for the mid-span and near tip regions, which when even optimized, deliver much greater SPL values than the root airfoils. It is apparent that geometries for these positions are very similar, with equal similarity in SPL values and it is relevant to point out the major decrease in aerodynamic performance, with very little decrease in noise emission when comparing to the previous airfoils optimized to favour the C_l/C_d ratio.

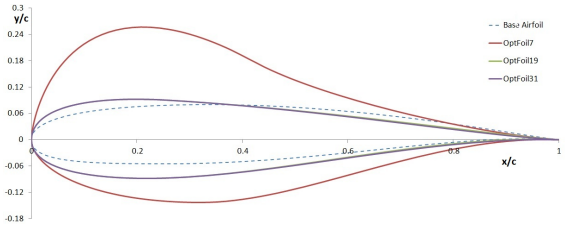

Figure 8. Optimized geometries, to assess the effect of radial position on noise levels

This first analysis is useful to identify that the airfoils integrated in the near tip regions are critical, which was apparent from the results for the reference airfoils, as these are likely to be the noisiest airfoils of all positions considered in the optimization tests. This is to be expected as rotational effects inherent to the flow around a WT are felt with increasingly effect as we consider the most exterior radial positions, relative to the root of the blade. For this reason, the following sections present the same kind of aerodynamic and aero-acoustic discussion for the near tip region radial position, where local flow speeds are certain to be higher and more interesting results may be achieved.

D. Effects of flow speed

The distance source-observer is fixed here at $250[m]$, and the remaining conditions are described in Tab.5.

Table 5. Constant parameters used for obtaining OptFoils 25, 29, 27 and 31

$r/R = 0.90$	$r_e = 250.0[m]$			
Parameter/OptFoil	25	29	27	31
U	15		20	
c [m]	0.8			
x	6.3			
L [m]	1.6			

The resulting geometries from the variation in flow speed, with the objective function set for maximizing C_l/C_d are presented in Fig.9. The difference in geometric properties are notorious between the airfoils

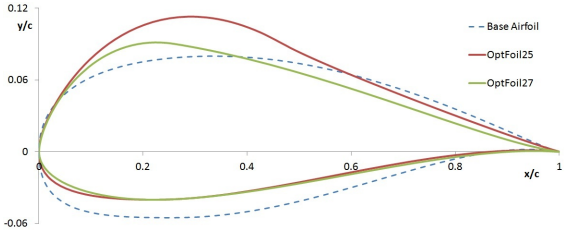

Figure 9. Optimized geometries to assess the effect of flow speed on aerodynamic performance

displayed, being once more the geometry with bigger thickness distribution the one with higher C_l/C_d ratio, even at a lower flow speed considered. The increase in $5[m.s^{-1}]$ from OptFoil 25 to OptFoil 27 aggravates the total noise level, with no gain in aerodynamic performance. Geometrically, OptFoil 27 presents a maximum thickness point closer to the LE, but the pressure side of the airfoil seems to allow the creation of negative aerodynamic effects in that section. In conclusion, the increase in flow speed affected negatively aerodynamic performance and SPL value.

The geometries obtained to minimize noise are as presented in Fig.10. The geometries present very similar overall shapes, acquiring an almost tear like surface and, presenting a similar evolution in geometry to that observed previously when accounting for the effects of radial position. Ultimately, with increasing speed flow, so do SPL values increase. Both geometries develop very similar low aerodynamic properties, but the most interesting aspect is the direct comparison to the previous geometries displayed in Fig.9. There is a general agreement when comparing f_1 and f_2 values for the corresponding geometries working under the

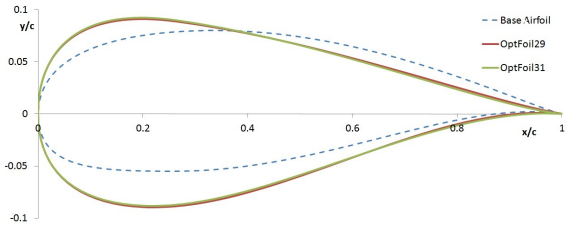

Figure 10. Optimized geometries, to assess the effect of flow speed on noise levels

same flow speed conditions. The difference from considering aerodynamically to aero-acoustically optimized airfoils, seems to translate in a major loss in lift (a relative difference of -90%) and a slight increase in drag (around 10% more) for a maximum minimization of SPL values in the order of 4 dB(A), when considering these working conditions.

E. Variation of the source-observer distance

The variation of the source-observer distance affects only the total SPL values computed, so only f_2 is here analyzed, but its sensitivity analysis and effect observed in the final optimized geometries will allow to assert how the airfoil geometries evolve when minimizing f_2 and help to account for any consistencies. For the fixed parameters $r/R = 0.90$ and $U = 20.0[m.s^{-1}]$, the test conditions are summarized in Tab.6.

Table 6. Constant parameters for airfoils 31 and 32

$r/R = 0.90\ U = 20.0[m.s^{-1}]$		
Parameter/OptFoil	31	32
r_e	250	1000
U	20	
c [m]	0.8	
x	6.3	
L [m]	1.6	

Figure 11 shows the effects of considering $r_e = 250$ and $1000[m]$. The main conclusion we can take from

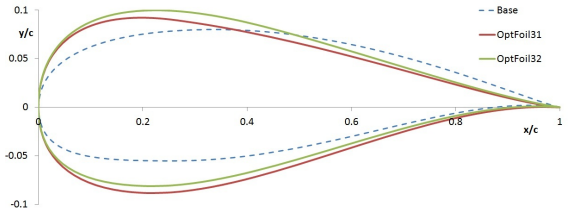

Figure 11. Optimized geometries, to assess the effect of source-observer distance on noise levels

this effect, apart from the obvious fact that greater distances considered deliver smaller values of SPL, is that the overall geometries of the airfoils optimized to minimize f_2 follow a very similar trend in evolution of geometry, maintaining from one effect analysis to the next a tear like shape, quite symmetrical with a slight S-tail shape of the TE. This last feature may be related with TE bluntness noise, as it requires that the TE wedge angle to be as small as possible, which does not allow the optimizer to develop a completely symmetrical airfoil. In any case, this detail in geometry evolution is good representation of the commitment of the optimizer in minimizing SPL values, since TE bluntness noise is not expected to be of major relevance in comparison to other noise mechanisms. This leads to the conclusion that this type of geometries are the ones to more likely develop smaller amounts of SPL values in complete detriment of aerodynamic performance.

F. Multi-objective optimization

After careful deliberation on the effects of the main parameters that can exert influence in the optimized geometries, it is of great relevance to study how the airfoil geometries evolve when considering the option to both maximize aerodynamic performance and minimize noise levels. For that purpose, MOO performed.

From the optimization performed, the Pareto front was built as illustrated in Fig.12 and five geometries were selected to analyze the best compromise between both objective functions as summarized in Tab.7.

Table 7. Optimization results for OptFoils 38 to 42

OptFoil	38	39	40	41	42
t/c	0.18	0.18	0.18	0.16	0.16
Ψ [deg]	9.9	11.6	15.6	12.6	10.4
C_l	0.3837	0.9796	1.2546	1.2853	1.3696
C_d	0.0068	0.0071	0.0079	0.0066	0.0066
SPL_T [dB(A)]	61.5	61.7	62.3	63.6	63.9
α^*	0.22	4.97	7.18	7.59	8.57
f_1^*	56.6	137.4	159.2	195.9	207.2
f_2^*	61.5	61.7	62.3	63.6	63.9

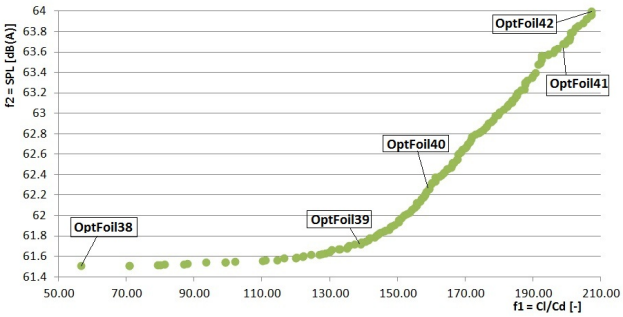

Figure 12. Pareto front for the MOO with $U = 20[m.s^{-1}]$, $r_e = 250.0[m]$ and $r/R = 0.90$

It is clear from Fig.12 that two classes of airfoil geometries can be distinguished, being one in the lower region of the curve, where SPL values are kept minimal but a great increase in C_l/C_d ratio can be achieved, and another region where higher SPL values must be considered for corresponding higher C_l/C_d ratios.

The geometries that comprise the first region are presented in Fig.13. The major geometrical difference between them is the variation in the TE region, specially for the suction side as the thickness distribution in that sector of the airfoil, seems to be bigger for the geometries that present an increase in f_1 whereas the thinner airfoils in that section deliver lower SPL values. That slight difference in aerodynamic performance is better acknowledged in the pressure distribution of the said geometries, as seen in Fig.14. The 1/3 octave

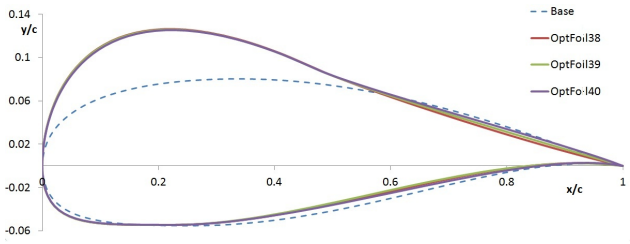

Figure 13. Pareto front for the MOO with $U = 20[m.s^{-1}]$, $r_e = 250.0[m]$ and $r/R = 0.90$

spectra of these geometries is presented in Fig.15 where the major difference seems to occur in the frequency range from 200 to 3000 Hz, which suggests a relation with the separated flow over the TE.

In another analysis of the second region identified in the Pareto front, the geometries shown in Fig.16 that maximize aerodynamic performance present more differences in shape between them than before, with emphasis in the x-coordinate of the maximum relative thickness point, being further away from the LE and

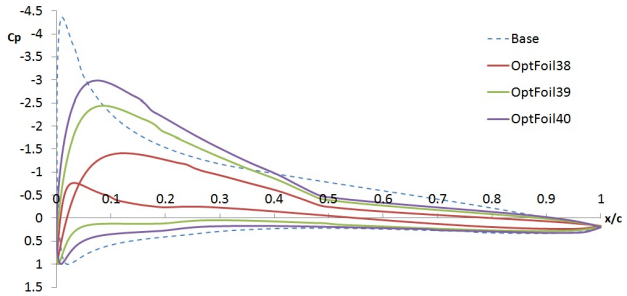

Figure 14. Pressure distribution of the optimized airfoils that minimize SPL value

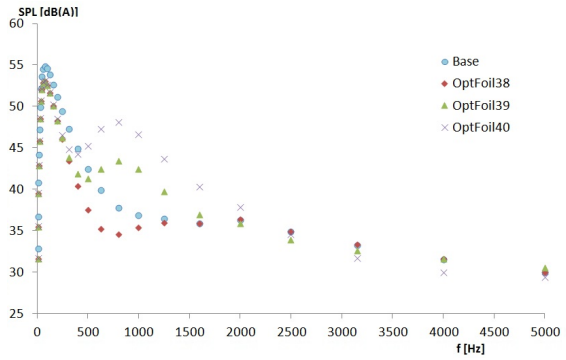

Figure 15. 1/3 octave spectra for the optimized arfoils that minimze SPL values

an obvious decrease in overall thickness distribution. The shape of the LE is very relevant to point out as

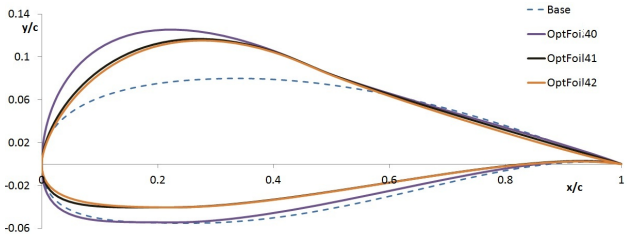

Figure 16. Optimized airfoils that maximize C_l/C_d ratios

the decrease in relative thickness may have had negative effects in total SPL value, namely through a bigger influence from turbulent inflow noise. The pressure distribution shown in Fig.17 shows that both geometries develop similar aerodynamic properties, but the difference in area towards the previously analyzed airfoils is sufficient for an increase in C_l/C_d ratio. Considering the opposing geometries selected from the Pareto front, the C_l/C_d ratio is increased in 72% at the cost of a relative SPL increase of nearly 4%. Figure 18 shows similar behavior developed by the previously analyzed geometries, with the main difference in SPL values being observed in the range of 500 to 3000 Hz, again possibly related with bigger influence from turbulent inflow noise.

The MOO presented is a major source of information on the optimized geometries. If one wants to minimize noise levels as much as possible, a geometry from the first region of the Pareto front is more suitable, with no significant penalization in the total SPL value, when changing the TE section. If instead, the gain in C_l/C_d is to be favoured, then a geometry taken from the second region of the same Pareto front is more adequate, with better corresponding total SPL values as changes are introduced in the LE and upper rear half section of the airfoil.

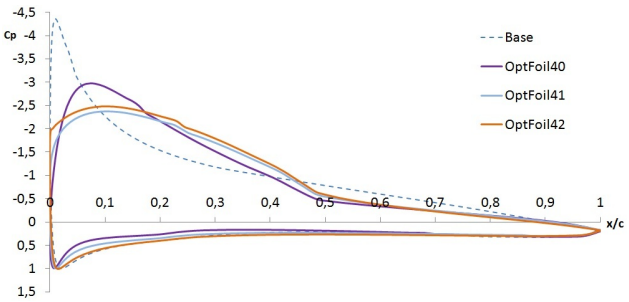

Figure 17. Pressure distribution for the optimized airfoils that maximize C_l/C_d ratios

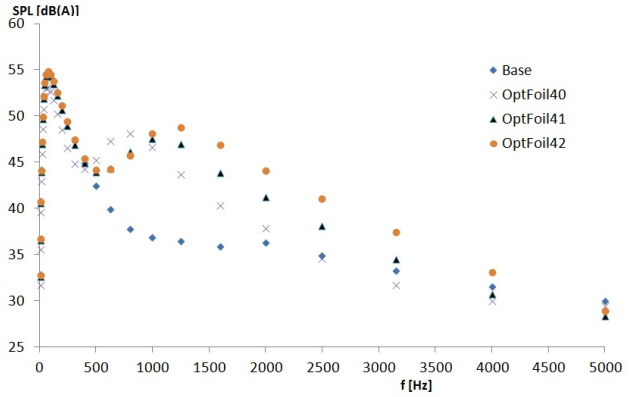

Figure 18. 1/3 octave spectra for the optimized airfoils that maximize C_l/C_d ratios

V. Conclusions

The multi-disciplinary optimization framework developed constitutes a powerful tool for the conceptual design stage of WT aifoils, handling both aerodynamic and aeroacoustics. The noise prediction scheme and optimization framework is not considered to be computationally too demanding, without compromising the reliability of the results.

The main results demonstrate that airfoil geometry design has a direct relation with several parameters that can be studied and analyzed to achieve the most satisfactory aerodynamic and aero-acoustic trade-off, depending on the objective intended.

Future developments include the use of gradient-based optimization algorithms for local refinement and the extension to three dimensional domains to account for the entire blade geometry. The inclusion of additional disciplines such as structures or more relevant objective functions such as cost of electric power output of the WT are also under consideration.

Acknowledgements

The author would like to leave here a word of recognition to Dr. Ruben E. Perez (Royal Military College of Canada) for precious help provided on using pyOpt, Dr. Peter J. Eecen (ECN Wind Energy) who kindly provided the Rfoil software and Patrick J. Moriarty (Senior Engineer at the National Wind Technology Center) for providing important explanations and documents on some of the subjects handled.

References

[1]WWEA, "World Wind Energy Report," Technical report, World Wind Energy Association, Bonn, Germany, April 2011, 10^{th} World Wind Energy Conference & Exhibition, Cairo, Egipt.

[2]Colby, W. D., Dobie, R., Leventhall, G., Lipscomb, D. M., McCunney, R. J., Seilo, M. T., and Sondergaard, B., "Wind

Turbine Sound and Health Effects An expert Panel Review," Technical report, American Wind Energy Association and Canadian Wind Energy Association, December 2009.

[3]Bertagnolio, F., Sorensen, N., Johansen, J., and Fuglsang, P., "wind Turbine airfoil catalogue," Tech. Rep. ISBN: 87 550 2910, Riso National Laboratory, August 2001.

[4]Timmer, W. A. and van Rooij, R. M., "Summary of the DELFT University Wind Turbine dedicated airfoils," Tech. Rep. AIAA-2003-0352, Delft University Wind Energy Research Institute, Stevinweg, The Netherlands, 2003.

[5]Samareh, J. A., "A survey of shape parameterization techniques," NASA, Hampton, VA, USA, June 1999, pp. 333–343.

[6]Grasso, F., *Multi-Objective Numerical Optimization applied to Aircraft Design*, Doctoral thesis, Universitá degli Studi di Napoli "Fedrico II", Facoltá Ingegneria, Dipartimento Ingegneria Aerospaziale, December 2008.

[7]Derksen, R. W. and Rogalsky, T., "Bezier-Parsec: An optimized aerofoil parameterization for design," *Advances in engineering software*, , No. 41, April 2010, pp. 923–930.

[8]V., P. and Lal, S. A., "Bezier Parameterization of an airfoil using genetic algorithm," 2010, Department of Mechanical Engineering, College of Engineering, Thiruvananthapuram, Kerala, India.

[9]Montgomerie, B. O., Brand, A. J., Bosschers, J., and van Rooij, R. P., *Three Dimensional Effects in Stall*, ECN, June 1997.

[10]Drela, M. and Youngren, H., "XFOIL 6.94 User Primer," Software Documentation, December 2001, Latest update.

[11]Brooks, T. F., Pope, D. S., and Marcolini, M. A., "Airfoil Self-Noise and Prediction," Reference Publication 1218, National Aeronautics and Space Administration, USA, July 1989.

[12]Moriarty, P. J., Guidati, G., and Migliore, P., "Recent improvement of a semi-empirical Aeroacoustic prediction code for Wind Turbines," 10^{th} *AIAA/CEAS Aeroacoustics Conference*, No. AIAA 2004-3041, 2004, Manchester, UK.

[13]Moriarty, P. J., Guidati, G., and Migliore, P., "Prediction of turbulent inflow and trailing edge noise for wind turbines," Technical report, American Institute of Aeronautics and Astronautics, 2005.

[14]Amiet, R., "Acoustic radiation from an airfoil in a turbulent stream," *Journal of Sound and Vibration*, Vol. 41, No. 4, 1975, pp. 407–420.

[15]Lowson, M. V., "Assessment and prediction of Wind Turbine Noise," , No. ETSU W/13/00284/REP, 1993.

[16]Zhu, W. J., Heilskov, N., Shen, W. Z., and Sorensen, J. N., "Modelling of aerodynamically generated noise from wind turbines," Technical reoprt, Technical University of Denmark, DK-2800 Lyngby, Denmark, June 2005, Contributed by the Solar energy division of the ASME.

[17]Drela, M., *Frontiers of Computational Fluid Dynamics*, chap. Pros and cons of airfoil optimization, No. ISBN 981-02-3707-3, World Scientific, 1998.

[18]Perez, R. E. and Jansen, P. W., *pyOpt Reference*, Python Software Foundation, release 1.0.1 ed., June 2011.

[19]Moriarty, P., *NAFNoise User's Guide*, National Wind Technology Center, National Renewable Energy Laboratory, USA, Golden, Colorado, July 2005.

[20]Dahl, K. S. and Fuglsang, P., "Design of the Wind Turbine Airfoil Family Riso-A-XX," Tech. rep., December 1998.